CLIMATOLOGY

Human-caused Indo-Pacific warm pool expansion

10.1126/sciadv.1501719

Evan Weller,[1] Seung-Ki Min,[1]* Wenju Cai,[2,3] Francis W. Zwiers,[4] Yeon-Hee Kim,[1] Donghyun Lee[1]

The Indo-Pacific warm pool (IPWP) has warmed and grown substantially during the past century. The IPWP is Earth's largest region of warm sea surface temperatures (SSTs), has the highest rainfall, and is fundamental to global atmospheric circulation and hydrological cycle. The region has also experienced the world's highest rates of sea-level rise in recent decades, indicating large increases in ocean heat content and leading to substantial impacts on small island states in the region. Previous studies have considered mechanisms for the basin-scale ocean warming, but not the causes of the observed IPWP expansion, where expansion in the Indian Ocean has far exceeded that in the Pacific Ocean. We identify human and natural contributions to the observed IPWP changes since the 1950s by comparing observations with climate model simulations using an optimal fingerprinting technique. Greenhouse gas forcing is found to be the dominant cause of the observed increases in IPWP intensity and size, whereas natural fluctuations associated with the Pacific Decadal Oscillation have played a smaller yet significant role. Further, we show that the shape and impact of human-induced IPWP growth could be asymmetric between the Indian and Pacific basins, the causes of which remain uncertain. Human-induced changes in the IPWP have important implications for understanding and projecting related changes in monsoonal rainfall, and frequency or intensity of tropical storms, which have profound socioeconomic consequences.

INTRODUCTION

The Indo-Pacific warm pool (IPWP), where sea surface temperatures (SSTs) exceed 28°C (which is an estimated threshold for atmospheric deep convection), supports the Walker circulation's rising branch and largely determines rainfall distribution throughout the tropics to extratropics (*1*, *2*). It plays a key role in climate and monsoon variability for many developing countries throughout Asia and Africa (*3*–*7*), but also influences remote regions and large-scale climate modes of variability (*8*–*10*). From year to year, IPWP intensity and size fluctuate with the El Niño–Southern Oscillation (ENSO) (*5*, *11*–*13*). The ongoing IPWP warming and expansion in recent decades (*5*, *7*, *11*, *12*) (Fig. 1A) are, by one estimate, responsible for more tropical Indo-Pacific SST variance than anomalies associated with ENSO (*5*).

Recent studies suggest greenhouse gas–induced warming to be the major cause for global ocean temperature (*14*) and tropical Indian Ocean SST changes (*12*, *15*–*17*), but its role in the observed IPWP region changes (*14*, *16*, *17*) is not clear. We provide the first quantitative attribution of the observed IPWP warming and expansion changes during the past 60 years, examining anthropogenic and natural contributions to the IPWP warming and expansion. We address this by comparing observed 1953–2012 changes with climate model–simulated changes using CMIP5 (Coupled Model Intercomparison Project Phase 5) (*18*) historical climate change simulations that account for anthropogenic forcing (greenhouse gases, aerosols, and other anthropogenic forcing agents) combined with natural (solar and volcanic activities) forcings (ALL), greenhouse gas forcing only (GHG), or natural forcings only (NAT).

[1]School of Environmental Science and Engineering, Pohang University of Science and Technology, Pohang 37673, South Korea. [2]Commonwealth Scientific and Industrial Research Organisation Marine and Atmospheric Research, Aspendale, Victoria 3195, Australia. [3]Physical Oceanography Laboratory, Qingdao Collaborative Innovation Center of Marine Science and Technology, Ocean University of China, Qingdao 266071, China. [4]Pacific Climate Impacts Consortium, University of Victoria, Victoria, British Columbia V8W 2Y2, Canada.
*Corresponding author. Email: skmin@postech.ac.kr

RESULTS

Observed and modeled changes

Models simulate the observed Indo-Pacific warming and IPWP expansion (Fig. 1B) reasonably well, albeit with greater warming and expansion in the central to eastern Pacific (fig. S1), a region affected by persistent biases (for example, excessively strong equatorial Pacific cold tongue) (*19*). We focus our analysis on 29 of 42 models (tables S1 and S2; see Materials and Methods) that simulate a realistic IPWP (that is, comparable size to observations; fig. S2) to reduce the impact of biases because there is a close relationship between IPWP mean size with changes in intensity and area (fig. S3). Specific forcing experiments show that realistic changes occur only when greenhouse gases are included (Fig. 1, B to D) but that the response is stronger than observed in GHG-only experiments, which exclude negative contributions from other anthropogenic forcings, such as aerosols (*16*, *17*).

To examine long-term IPWP intensity and area changes, we considered nonoverlapping 5-year annual means over the 60-year period. Mean IPWP SST and area are calculated over the Indo-Pacific region enclosed by the 28°C isotherm between 25°S to 25°N and 40°E to 130°W. We also independently analyze the Indian and Pacific Ocean warm pools (Fig. 1A). The IPWP warmed and expanded steadily until the late 1990s, followed by weaker trends, as observed in global mean temperature (Fig. 2) (*20*). The ALL and anthropogenic forcing (ANT; estimated as ALL minus NAT) simulations show realistic increasing trends, whereas GHG-only trends are significantly larger than observed. In contrast, NAT-only simulations have varying decadal trends, resulting in no significant long-term trend. The signal induced by ANT-only is therefore close to that from ALL forcing (Table 1). Preindustrial control simulations from the models are used to provide a measure of the range of trends arising from unforced internal climate variability, which the observed trends exceed (Fig. 2).

Despite studies reporting tropical Indian Ocean warming at a rate of up to three times faster than the tropical Pacific (fig. S4A) (*5*, *12*, *17*, *21*), trends are comparable if only area-mean SSTs averaged in the expanding warm pool of both oceans are compared, due to the larger increase in warm pool size in the Indian Ocean (Fig. 2 and Table 1). Therefore,

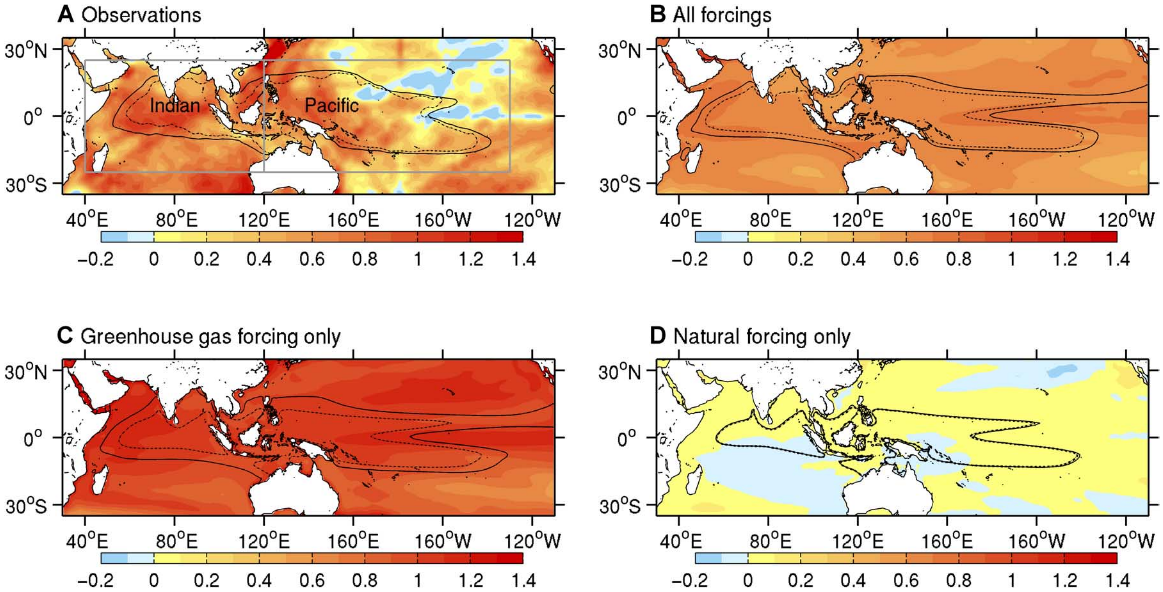

Fig. 1. Geographical distribution of SST trends and warm pool expansion over the Indo-Pacific during 1953–2012. (**A** to **D**) HadISST (*39*) observations (A) and CMIP5 (*18*) multimodel means for each type of forcing: (B) anthropogenic plus natural external (29 models), (C) greenhouse gas only (6 models), and (D) natural external only (6 models). In each panel, trends are °C per 60 years, and the mean IPWP area is shown for two periods: 1953–1959 (dashed line) and 2000–2012 (solid lines). Gray boxes in (A) depict the area over which warm pool regions are calculated for the IPWP, divided into Indian and Pacific sectors by the 120°E meridian.

the zonal intensity gradient (Indian minus Pacific) between the two warm pool sectors has experienced little change (fig. S4B). Year-to-year variations of approximately 10 to 15% (relative to the climatological mean) in IPWP size occur with ENSO (*12*, *13*, *22*), far less than the observed expansion of over 30% since the 1950s (Fig. 2B and Table 1). Warm pool expansion in the Indian Ocean (51%) has also far exceeded that in the Pacific Ocean (22%) (Fig. 2B and Table 1). These results are consistent among observational data sets despite some regional differences, and are different to similar expansion rates in both basins associated with a uniform warming (fig. S5).

Detection of human influence

To detect and quantify contributions from ALL, GHG, ANT, and NAT forcings to long-term variations in IPWP intensity and area, we use an optimal fingerprinting technique (*23*). In this method, observations are regressed via generalized linear regression onto one or two multimodel-simulated signals (see Materials and Methods for details). We conduct single-signal analyses by regressing observations onto model-simulated responses to ALL, ANT, GHG, and NAT forcings estimated from the average of the selected model ensemble. We conduct a two-signal analysis in which observations are simultaneously regressed onto ANT and NAT response to estimate the contribution of both anthropogenic and natural forcings to changes in warm pool properties. Unforced control (CTL) simulations are used to obtain an estimate of the internal climate variability, in addition to conducting a residual consistency test (*23*) to compare model-simulated internal variability with observations. Resulting best estimates and uncertainty ranges of scaling factors, which scale estimates of the responses to individual combinations of forcings to best reproduce observed changes, are used to determine whether external forcings are present in observations. Intensity and area changes are not perfectly correlated ($r = 0.87$, $P < 0.01$), and thus, we combine normalized intensity and area anomalies to capture additional information on changes that may improve detection and attribution (*24*). The influence of external forcing is detected when a scaling factor is significantly greater than zero, and considered consistent with observations when it is consistent with unity.

Scaling factors based on single-signal optimal analyses are shown in the left panels of Fig. 3. Except for the Pacific warm pool area, scaling factors for ALL, GHG, and ANT are significantly greater than zero for long-term warm pool intensity and area changes, including combined changes. This indicates that the overall effect of external anthropogenic and natural forcing, or the effect of greenhouse gas forcing or anthropogenic forcing alone, can be detected. In most cases, uncertainty ranges for the scaling factors on the ALL and ANT responses include unity, indicating consistency with observations. Best estimates for ALL and ANT scaling factors are slightly above one for warm pool intensities and Indian Ocean warm pool area (Fig. 3, A and B), highlighting some underestimation of the response in the multimodel mean. In contrast, best estimates for GHG are below one, meaning that GHGs acting alone would have produced larger changes than the observed. Strong agreement of best estimates with observed trends is found in all three warm pool regions when combining intensity and area changes (Fig. 3C). The influence of NAT is not robustly detected in any case considered. The residual consistency test is passed in most of the single-signal cases, indicating that the residual variability that remains in the observations after removing the scaled response is consistent with model internal variability.

Results from two-signal (ANT and NAT) analyses of warm pool intensity and area changes are shown in the center panels of Fig. 3. The ANT influence is detected in all cases with clear separation from the NAT influence except for the Pacific warm pool area. The ANT scaling factors for IPWP changes are closest to unity with more confidence compared to the Indian and Pacific Oceans separately. Overall, ANT signals for warm pool intensity must be scaled up, and ANT signals

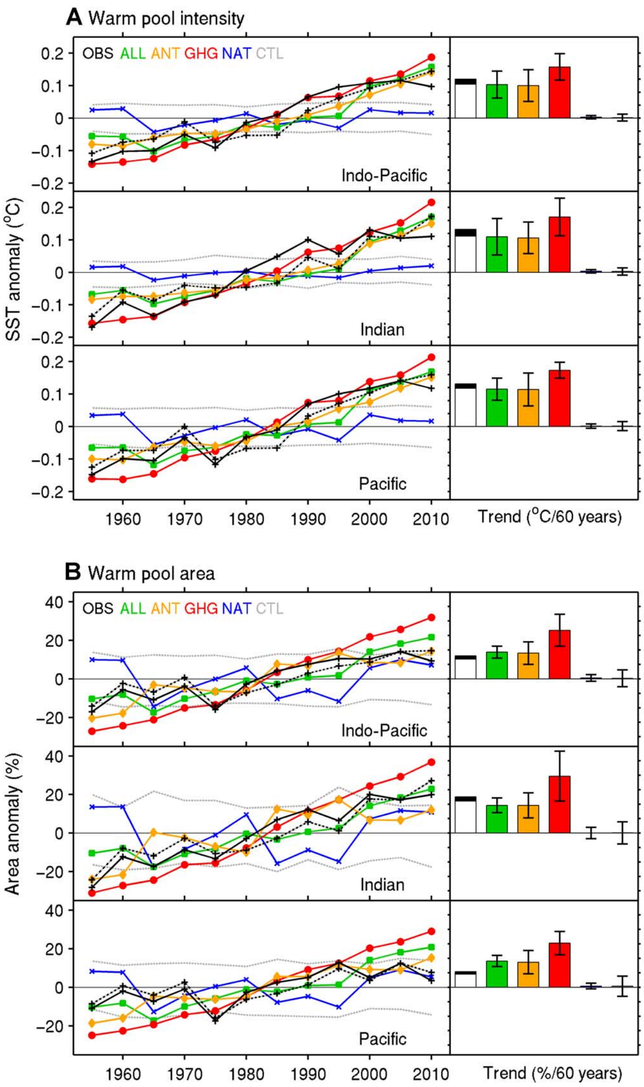

Fig. 2. Time series of 5-year mean anomalies of warm pool intensity and area. (**A**) Observed (*39*) (black) SST anomalies (°C) with (solid) and without (dashed) PDO influence are compared with multimodel mean–simulated responses to anthropogenic plus natural external forcings (ALL; green), anthropogenic forcing (ANT; calculated as ALL minus NAT; orange), greenhouse gas only forcing (GHG; red), and natural external only forcings (NAT; blue) for the Indo-Pacific (top), Indian Ocean (center), and Pacific Ocean (bottom) warm pools. Gray dashed lines represent the 5 to 95% range of internal variability taken from control (CTL) simulations. Linear trends [error bars representing 5 to 95% confidence intervals (CIs)] for observations with (black) and without (white) PDO and multimodel mean over the period 1953–2012 are displayed to the right. (**B**) The same as (A) but for warm pool area anomalies (as a percentage of each 1971–2000 mean) in the three warm pool regions.

for warm pool area need to be scaled up for the Indian Ocean, but CIs encompass unity. NAT is not robustly detected because the joint confidence ellipses include zero on the NAT axis in all cases.

ANT-attributable trends (calculated by multiplying two-signal scaling factors with multimodel mean trends) are very close to observed intensity (Fig. 3A) and area (Fig. 3B) trends. Considering combined changes increases the "detection strength," which is a representation of the projection of any model run or observations onto the single variable or combined fingerprint (*24*), and further increases confidence that intensity and area changes are not due to internal variability alone (Fig. 3C). Our detection results are robust to the use of different SST data sets and different model sampling (see Materials and Methods).

Internal variability influence

To understand the models' underestimation of the warm pool warming, we assess the contribution of internal climate variability evident in observations (Fig. 2). The dominant mode of multidecadal variability in the Indo-Pacific is the Pacific Decadal Oscillation (PDO) (*25*). Changes in IPWP intensity and area associated with the observed PDO variability during the last 60 years have augmented that due to anthropogenic forcing. The contribution of the PDO to the observed IPWP warming and expansion is approximately 12 to 18% (Table 1). Removing the PDO influence from observations (based on linear regression) results in better agreement with multimodel anthropogenic responses in intensity trends and Indian Ocean warm pool expansion (Fig. 2) (*26*, *27*).

Impact of IPWP changes

We investigate the impact of the nonuniform IPWP changes focusing on rainfall responses using observations and CMIP5 models. On the basis of the observations for the satellite period, different rainfall change patterns appear to be more associated with individual Indian and Pacific warm pool changes than for the IPWP as a whole (fig. S6). This emphasizes the importance of the regional IPWP warming patterns in terms of IPWP's impacts and teleconnections. Satellite period observations show more warming and larger expansion in the Indian Ocean warm pool than in the Pacific, together with an intensification and westward shift in precipitation change, even after accounting for the influence of internal variability during this period (fig. S7, A and B). The notion that the asymmetric response in the IPWP changes is not due to fluctuations of internal variability is supported by the CMIP5 models because they exhibit no relationship between the ratio of Indian and Pacific warm pool expansion with the PDO trend over a 60-year period (fig. S7C). We use CMIP5 models to further explore the individual impacts of Indian and Pacific Ocean warm pool warming and expansion on rainfall. To do so, we have selected two groups of models: one with trends in IPWP intensity and area similar to those observed, that is, with stronger warming and expansion trends in the Indian Ocean than in the Pacific Ocean (five models; refer to caption in fig. S8), and another group with opposite trends (six models). Note that we use a longer period of 1953–2012 to focus on long-term responses, different from the observed period (1979–2012).

Regional precipitation patterns are determined by relative changes in the spatial pattern of the tropical SST climatology (*28*–*30*). Given the large intermodel differences in tropical SST climatology and trends, one cannot expect good intermodel agreement in rainfall responses (*28*, *31*). Accordingly, our results show generally low agreement in rainfall trends except in a few regions (fig. S8). In particular, models with larger expansion in the Indian Ocean, like the recent observations, tend to have increased rainfall over the western Indian Ocean that resembles the observed trend. In contrast, models with stronger warm pool warming and expansion in the western Pacific exhibit a decrease in precipitation over Southeast Asia. This model-simulated drying response is consistent with previous findings (*32*, *33*), which describe the major role of zonal SST difference between the tropical Indian Ocean and western Pacific Ocean in determining the strength of the western

Table 1. Comparison of trends in warm pool intensity and area between observations and climate model simulations. Multimodel means of linear trend slopes are defined as the signal (S_{ALL}, S_{ANT}, S_{GHG}, or S_{NAT}), and the SD of trends across nonoverlapping CTL chunks is defined as the noise (N). The 5 to 95% CIs are shown in Fig. 2. Signal-to-noise ratios (SNRs) are then calculated from slopes of SST and area series averaged over the three warm pool regions during 1953–2012 for ALL and ANT simulations. Observational (39) trend slopes with (S_{OBS}) and without the influence of the PDO (S_{OBS*}) are given for comparison. Units for S and N are °C and % per 60 years for warm pool intensity and area, respectively.

	S_{ALL} (SNR_{ALL})	S_{ANT} (SNR_{ANT})	S_{GHG}	S_{NAT}	N_{CTL}	S_{OBS} S_{OBS}*
Intensity (°C per 60 years)						
Indo-Pacific	0.25 (7.24)	0.24 (7.01)	0.39	0.01	0.03	0.30 (0.26*)
Indian	0.26 (9.16)	0.25 (8.97)	0.43	0.01	0.03	0.34 (0.28*)
Pacific	0.28 (6.14)	0.27 (6.02)	0.43	0.01	0.05	0.33 (0.29*)
Area (percentage per 60 years)						
Indo-Pacific	37.3 (2.99)	35.3 (2.83)	67.1	2.0	12.5	32.2 (27.4*)
Indian	38.4 (2.1)	36.4 (1.99)	78.77	2.1	18.3	51.2 (44.3*)
Pacific	36.7 (2.36)	34.7 (2.23)	61.0	2.0	15.6	21.6 (18.0*)

Pacific subtropical high and thus affecting East Asian monsoon rainfall and western Pacific tropical cyclone activity. Australian rainfall response in models is also consistent with recent findings (*34*), which indicate that a warming Indian Ocean warm pool induces rainfall increase, whereas a warming Pacific warm pool leads to rainfall reduction (fig. S8). The spatial pattern of difference in rainfall trends between the two model groups (models with larger expansion in the Indian Ocean minus models with larger expansion in the Pacific Ocean) is very similar to the observed pattern of trends (compare fig. S8C with fig. S7), confirming the importance of the area of SST contrast between the two warm pool areas. The individual models help highlight the large spread that still exists in models with similar changes in expansion of the IPWP, explaining why we see only limited regions of significant change (fig. S8D). For example, the difference in the western Indian Ocean is significant (at the 1% level) between the two model groups because the realistic models all simulate the increase in rainfall. Conversely, the opposite is seen for the East Asian region, where models that simulate larger Pacific expansion have a decrease in rainfall, again consistent with previous modeling studies, which showed that a significant drying response over East Asia is primarily associated with stronger Pacific warming (*32*, *33*). Consistent with the observations, the ensemble mean of models with the more realistic larger Indian Ocean expansion does not simulate an increase in the East Asia region. In the observations, the small significant region of drying over East Asia is removed once the PDO is accounted for (fig. S7). This corroborates previous findings that the negative PDO-like SST pattern that prevailed during the recent hiatus period explains pronounced regional drying anomalies in this region (*33*).

Regions of deep convection are integral to the large-scale circulation in the tropics and closely tied to areas of warm SSTs (*35*, *36*). However, the size of this region of convection has been shown to remain relatively constant in a warming world, suggesting that the convective threshold increases with SST and that precipitation intensity increases within the region that lies above the changing convective threshold (*11*, *36*). We have therefore also examined convection changes that correspond to IPWP changes based on a simple analysis of CMIP5 models. We find that rainfall intensity modestly increases with warming in the IPWP in most of the models, but the convection area (diagnosed as the area with precipitation > 2 mm day^{-1}) changes very little (fig. S9). In contrast to the warm pool expansion, both basins experience a similar increase in warm pool intensity, and thus, simulated changes in precipitation increase as described in previous studies (*11*, *37*) and as observed. Overall, although the convection area does not vary significantly in the long term as the convection threshold increases with SST, covering about 25% of the global ocean (*11*), its location has undergone a significant shift westward with a relatively larger area with SSTs above the convection threshold in the Indian Ocean.

DISCUSSION

Our results identify contributions from anthropogenic forcings (mainly greenhouse gas increase) and natural causes (the PDO) to observed IPWP warming and expansion during the last 60 years. This quantitative attribution of the influence of anthropogenic forcing and also assessment of climate variability increases confidence in the understanding of the causes of past changes as well as for projections of future changes under further greenhouse warming. Expansion of the IPWP due to anthropogenic forcing will likely continue; however, shifts in the mean state of the tropical ocean (*13*, *20*, *21*, *26*) could change the relative amounts of expansion in the two adjacent oceans and modulate the long-term change in the IPWP impact. This has important implications for many vulnerable regions. For example, stronger than normal summer Indian monsoons are preceded by an expanding and warming Indian Ocean warm pool (*22*). A mean state change in this direction could also affect East Asian climate by inducing a westward extension of the western Pacific subtropical high (*3*). In addition to long-term trends, decadal variability in IPWP intensity and size can directly affect the Hadley and Walker circulations, inducing corresponding changes in rainfall even in the extratropics (*38*). This means that understanding and predicting changes of the IPWP mean state as well as regional con-

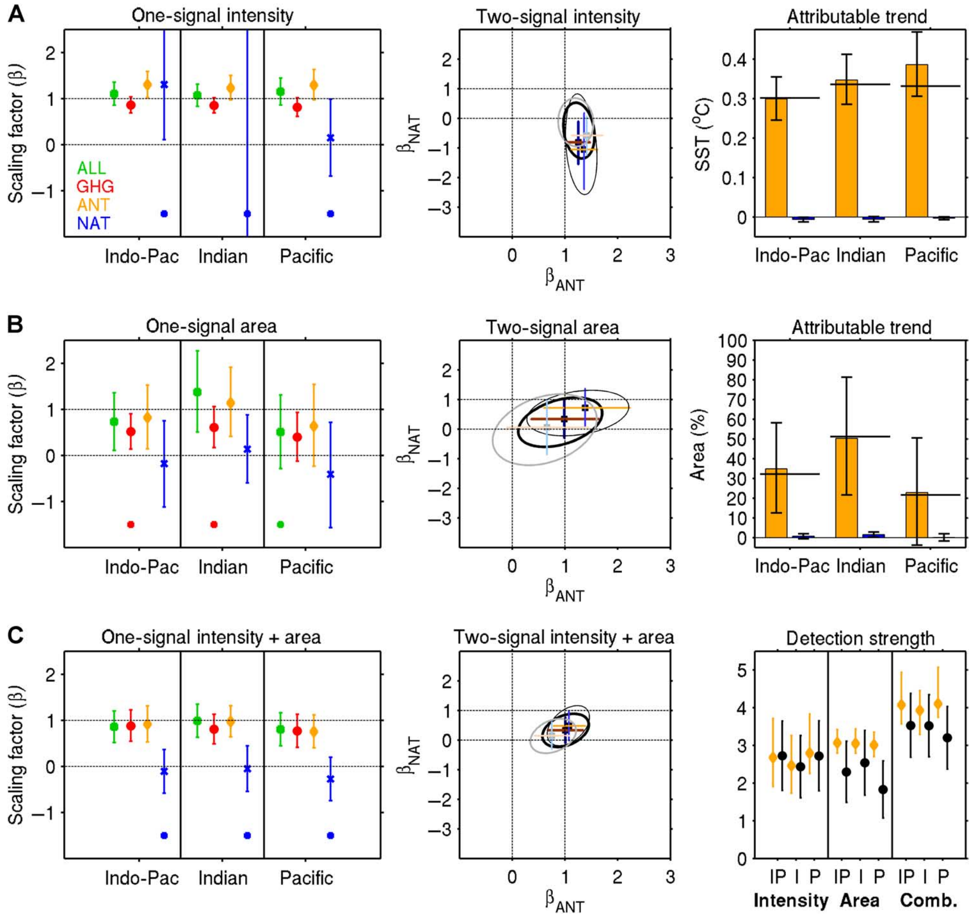

Fig. 3. Results from optimal detection analysis of warm pool intensity and area with corresponding attributable trends. (**A** to **C**) Scaling factors of warm pool SST (A), area (B), and combined SST and area anomalies (C) for single-signals of anthropogenic plus natural external (ALL; green), greenhouse gas only (GHG; red), anthropogenic (ANT; orange), and natural external only (NAT; blue) forcings (left), and for two signals of ANT (*x* axis) and NAT (*y* axis) (center). In two-signal panels, dark, medium, and light colors indicate the Indo-Pacific, Indian, and Pacific warm pools, respectively. Best estimates (data points) and 5 to 95% CIs (error bars) of scaling factors are displayed, and the 5 to 95% joint confidence for two signals are represented by ellipses. Detectable response to an individual forcing occurs when scaling factors are significantly greater than zero. Consistency between observed and simulated responses is determined when scaling factors are not significantly different from unity. Also shown in corresponding bar graphs (right) of (A) and (B) are ANT- and NAT-attributable intensity and area trends (bar and 5 to 95% CI) from two-signal analysis (center) compared to observed trends (horizontal solid lines). The right panel of (C) compares the detection strength (mean and 5 to 95% CI) of the multimodel fingerprint of ANT in model runs (orange) and observations (black).

trast is critical to reliable future projections of changes in global and regional atmospheric circulation and hydrological cycle (*1–4*, *6*, *7*, *10*, *32–34*, *38*).

MATERIALS AND METHODS

Data processing

We used SST from HadISST (Hadley Centre sea ice and SST) (*39*) v1.1 and ERSST (Extended Reconstructed SST) (*40*) v3b data sets for the period 1953–2012 to calculate properties of the IPWP (for example, intensity and area). The area enclosed by the 28°C isotherm for the Indo-Pacific sector between 25°S to 25°N and 40°E to 130°W was obtained using the monthly data. The mean seasonal cycle of intensity and area calculated for 1953–2012 was removed to obtain monthly anomaly information. Annual mean anomalies were constructed for analysis and comparison with model simulations. We assessed the relationship between warm pool properties (SST intensity and area greater than 28°C) and rainfall in the satellite era (1979–2012) with GPCP (Global Precipitation Climatology Project) monthly precipitation analysis (*41*) data.

We used 42 CMIP5 (*18*) models forced with historical anthropogenic and natural forcings (1953–2005) and future greenhouse gases under emission scenario of Representative Concentration Pathway (RCP) 4.5 (2006–2012), covering a 60-year period (table S1). The climatological size of the IPWP (area bounded by the 28°C isotherm) was used to select a subset of models. Of the 42 models, 29 satisfy the criterion whereby the size of the model's climatological IPWP lies within the observed average ± 1 SD of the observed interannual variability (fig. S2). The selected models yield a mean IPWP area of 46.0×10^{12} m^2, close to the observed area in HadISST of 43.9×10^{12} m^2 (table S2). In total, 80 simulations of the historical period were used, referred to as the ALL forcing experiment. Individual forcing simulations using greenhouse gases only (GHG-only) and external natural forcing only

(NAT-only) were obtained from the selected models (if available), with a total of 25 and 29 simulations, respectively.

All model outputs were regridded to a common 1° × 1° latitude/longitude grid, then ensemble means were first calculated for individual models, and multimodel means were obtained by taking arithmetic averages of the model-specific ensemble means, giving equal weight to each model when constructing multimodel means. We estimated the anthropogenic forced (ANT) signal as the difference between ALL and NAT under the assumption of linearly additive responses to the external forcings. Preindustrial control (CTL) simulations (19,800 years, which provided 333 nonoverlapping 60-year chunks in total) from all available models were used to estimate the characteristics of model unforced internal climate variability (Table 1) to increase number of independent noise data, which helps reduce sampling uncertainty in covariance estimation of the internal climate variability (*42*). Using CTL simulations from the 29 selected models did not affect main results.

Detection method

To compare observed and modeled warm pool intensity and area anomaly time series, an optimal fingerprinting technique (*23*) was used. Observations ($\mathbf{y}$) were regressed onto multimodel mean response patterns ($\mathbf{X}$, fingerprints of ALL, ANT, GHG, and NAT) such that $\mathbf{y} = (\mathbf{X} - \boldsymbol{\nu})\boldsymbol{\beta} + \boldsymbol{\varepsilon}$. Here, regression coefficients $\boldsymbol{\beta}$ (or scaling factors) are obtained by the total least squares method, $\boldsymbol{\nu}$ represents the component of $\mathbf{X}$ due to internal variability that remains after multimodel averaging, and $\boldsymbol{\varepsilon}$ represents the residual variability that is generated internally in the climate system. The variance-covariance matrix of $\boldsymbol{\varepsilon}$ is estimated from preindustrial control (CTL) simulations, and that of $\boldsymbol{\nu}$ is taken to be proportional to the variance-covariance matrix of $\boldsymbol{\varepsilon}$, where the constant of proportionality reflects the methods used to calculate the multimodel ensemble response patterns. We conducted two regression analyses. (i) Single-signal analyses were performed by linearly regressing observations onto single (ALL, ANT, GHG, or NAT) fingerprints to examine whether the signal considered is present in the observed changes. (ii) A two-signal analysis was undertaken whereby observations were regressed onto ANT and NAT simultaneously. This allows an examination of whether ANT and NAT are jointly detected and whether the influence of ANT is separable from that of NAT and internal variability in the observations. We divided 60-year chunks of CTL simulations into two sets (116 chunks each) for the optimal fingerprinting analysis. The first set was used to obtain best estimates of $\boldsymbol{\beta}$, and the other set was used to estimate the 5 to 95% uncertainty range for $\boldsymbol{\beta}$ and also to carry out a standard residual consistency test (*23*, *43*). This test offers a convenient method to check whether model-simulated internal variance is consistent with observational residual variance. Because the key aspect of this study was on long-term variability of warm pool intensity and area changes, we calculated 5-year mean time series of anomalies to reduce noise on interannual time scales. Therefore, 12-dimensional data vectors of observations and model simulations were obtained. Because data vectors have low dimension compared to the number of chunks of CTL simulations available for covariance matrix estimation (12 dimensions versus 115 chunks for each of the two covariance matrix estimates), we did not apply further dimension reduction, such as empirical orthogonal function truncations (*43*).

We assessed the sensitivity of different model samples to forcing signals and optimal fingerprinting analysis by using six models that had ALL, GHG, and NAT simulations. This evaluation also allowed an assessment of the sensitivity of the calculation of the anthropogenic forcing as the difference between ALL and NAT to the use of multimodel means from different samples of models. The results were found to be robust regardless of model samples used (compare Figs. 2 and 3 with figs. S10 and S11). For example, long-term trends (fig. S10) and scaling factors from optimal fingerprinting results (fig. S11) were found to be robust to the use of different multimodel ensembles.

SUPPLEMENTARY MATERIALS

Supplementary material for this article is available at http://advances.sciencemag.org/cgi/content/full/2/7/e1501719/DC1

fig. S1. Relationship of observed and simulated SST trends in the Indo-Pacific region with global mean temperatures during 1953–2012.
fig. S2. Simulated IPWP area and intensity.
fig. S3. Relationships between warm pool intensity and area.
fig. S4. Time series of tropical ocean and warm pool intensity and zonal gradient during 1953–2012.
fig. S5. Sensitivity of observed SST trends and warm pool expansion over the Indo-Pacific during 1953–2012 to data set.
fig. S6. Observed rainfall anomalies associated with warm pool intensity and area variations.
fig. S7. Observed rainfall trend during the satellite era and intermodel relationship between zonal contrast of warm pool expansion and Pacific decadal variability.
fig. S8. Simulated rainfall trends from two groups of CMIP5 models and their difference.
fig. S9. Intermodel relationships between trends in convection and the IPWP.
fig. S10. Sensitivity of simulated warm pool intensity and area anomalies to model samples.
fig. S11. Sensitivity of optimal detection results to model samples.
table S1. List of CMIP5 model simulations used in this study.
table S2. Performance of 42 CMIP5 models integrated with observed time-evolving changes in anthropogenic and natural forcings.

REFERENCES AND NOTES

1. J. Fasullo, P. J. Webster, Warm pool SST variability in relation to the surface energy balance. *J. Clim.* **12**, 1292–1305 (1999).
2. R. Neale, J. Slingo, The Maritime Continent and its role in the global climate: A GCM study. *J. Clim.* **16**, 834–848 (2003).
3. T. Zhou, R. Yu, J. Zhang, H. Drange, C. Cassou, C. Deser, D. L. R. Hodson, E. Sanchez-Gomez, J. Li, N. Keenlyside, X. Xin, Y. Okumura, Why the western Pacific subtropical high has extended westward since the late 1970s. *J. Clim.* **22**, 2199–2215 (2009).
4. H. Annamalai, J. Hafner, K. P. Sooraj, P. Pillai, Global warming shifts the monsoon circulation, drying south Asia. *J. Clim.* **26**, 2701–2718 (2013).
5. A. P. Williams, C. Funk, A westward extension of the warm pool leads to a westward extension of the Walker circulation, drying eastern Africa. *Clim. Dyn.* **37**, 2417–2435 (2011).
6. M. Hoerling, J. Hurrell, J. Eischeid, A. Phillips, Detection and attribution of twentieth-century northern and southern African rainfall change. *J. Clim.* **19**, 3989–4008 (2006).
7. S. B. Ratna, A. Cherchi, P. V. Joseph, S. K. Behera, B. Abish, S. Masina, Moisture variability over the Indo-Pacific region and its influence on the Indian summer monsoon rainfall. *Clim. Dyn.* **46**, 949–965 (2016).
8. M. Hoerling, A. Kumar, The perfect ocean for drought. *Science* **299**, 691–694 (2003).
9. M. Hoerling, J. Eischeid, J. Perlwitz, X. Quan, T. Zhang, P. Pegion, On the increased frequency of Mediterranean drought. *J. Clim.* **25**, 2146–2161 (2012).
10. W. Han, J. Vialard, M. J. McPhaden, T. Lee, Y. Masumoto, M. Feng, W. P. M. de Ruijter, Indian Ocean decadal variability: A review. *Bull. Am. Meteorol. Soc.* **95**, 1679–1703 (2014).
11. C. D. Hoyos, P. J. Webster, Evolution and modulation of tropical heating from the last glacial maximum through the twenty-first century. *Clim. Dyn.* **38**, 1501–1519 (2012).
12. S. A. Rao, A. R. Dhakate, S. K. Saha, S. Mahapatra, H. S. Chaudhari, S. Pokhrel, S. K. Sahu, Why is Indian Ocean warming consistently? *Clim. Change* **110**, 709–719 (2012).
13. S.-K. Lee, W. Park, M. O. Baringer, A. L. Gordon, B. Huber, Y. Liu, Pacific origin of the abrupt increase in Indian Ocean heat content during the warming hiatus. *Nat. Geosci.* **8**, 445–449 (2015).
14. P. J. Gleckler, B. D. Santer, C. M. Domingues, D. W. Pierce, T. P. Barnett, J. A. Church, K. E. Taylor, K. M. AchutaRao, T. P. Boyer, M. Ishii, P. M. Caldwell, Human-induced global ocean warming on multidecadal timescales. *Nat. Clim. Chang.* **2**, 524–529 (2012).
15. M. K. Roxy, K. Ritika, P. Terray, S. Masson, The curious case of Indian Ocean warming. *J. Clim.* **27**, 8501–8509 (2014).

16. L. Dong, T. Zhou, The Indian Ocean sea surface temperature warming simulated by CMIP5 models during the twentieth century: Competing forcing roles of GHGs and anthropogenic aerosols. *J. Clim.* **27**, 3348–3362 (2014).
17. S.-L. Yao, G. Huang, R.-G. Wu, X. Qu, D. Chen, Inhomogeneous warming of the Tropical Indian Ocean in the CMIP5 model simulations during 1900–2005 and associated mechanisms. *Clim. Dyn.* **1**, 619–636 (2016).
18. K. E. Taylor, R. J. Stouffer, G. A. Meehl, An overview of CMIP5 and the experiment design. *Bull. Am. Meteorol. Soc.* **93**, 485–498 (2012).
19. G. Li, S.-P. Xie, Tropical biases in CMIP5 multimodel ensemble: The excessive equatorial Pacific cold tongue and double ITCZ problems. *J. Clim.* **27**, 1765–1780 (2014).
20. M. Watanabe, H. Shiogama, H. Tatebe, M. Hayashi, M. Ishii, M. Kimoto, Contribution of natural decadal variability to global warming acceleration and hiatus. *Nat. Clim. Chang.* **4**, 893–897 (2014).
21. J.-J. Luo, W. Sasaki, Y. Masumoto, Indian Ocean warming modulates Pacific climate change. *Proc. Natl. Acad. Sci. U.S.A.* **109**, 18701–18706 (2012).
22. S. T. Kim, J.-Y. Yu, M.-M. Lu, The distinct behaviors of Pacific and Indian Ocean warm pool properties on seasonal and interannual time scale. *J. Geophys. Res.* **117**, D05128 (2012).
23. M. R. Allen, P. A. Stott, Estimating signal amplitudes in optimal fingerprinting, part I: Theory. *Clim. Dyn.* **21**, 477–491 (2003).
24. D. W. Pierce, P. J. Gleckler, T. P. Barnett, B. D. Santer, P. J. Durack, The fingerprint of human-induced changes in the ocean's salinity and temperature fields. *Geophys. Res. Lett.* **39**, L21704 (2012).
25. N. J. Mantua, S. R. Hare, The Pacific Decadal Oscillation. *J. Oceanogr.* **58**, 35–44 (2002).
26. A. Dai, J. C. Fyfe, S.-P. Xie, X. Dai, Decadal modulation of global surface temperature by internal climate variability. *Nat. Clim. Chang.* **5**, 555–559 (2015).
27. G. P. Compo, P. D. Sardeshmukh, Removing ENSO-related variations from the climate record. *J. Clim.* **23**, 1957–1978 (2010).
28. S.-P. Xie, C. Deser, G. A. Vecchi, J. Ma, H. Teng, A. T. Wittenberg, Global warming pattern formation: Sea surface temperature and rainfall. *J. Clim.* **23**, 966–986 (2010).
29. R. Chadwick, I. Boutle, G. Martin, Spatial patterns of precipitation change in CMIP5: Why the rich do not get richer in Tropics. *J. Clim.* **26**, 3803–3822 (2013).
30. C. Liu, R. P. Allan, Observed and simulated precipitation responses in wet and dry regions 1850–2100. *Environ. Res. Lett.* **8**, 034002 (2013).
31. J. D. Neelin, M. Münnich, H. Su, J. E. Meyerson, C. E. Holloway, Tropical drying trends in global warming models and observations. *Proc. Natl. Acad. Sci. U.S.A.* **103**, 6110–6115 (2006).
32. B. Wang, B. Xiang, J.-Y. Lee, Subtropical High predictability establishes a promising way for monsoon and tropical storm predictions. *Proc. Natl. Acad. Sci. U.S.A.* **110**, 2718–2722 (2013).
33. H. Ueda, Y. Kamae, M. Hayasaki, A. Kitoh, S. Watanabe, Y. Miki, A. Kumai, Combined effects of recent Pacific cooling and Indian Ocean warming on the Asian monsoon. *Nat. Commun.* **6**, 8854 (2015).
34. L. Fan, S.-I. Shin, Z. Liu, Q. Liu, Two-sided impacts of warm pool SSTs in Australian precipitation changes. *Int. J. Climatol.* 10.1002/joc.4661 (2016).
35. K.-M. Lau, H.-T. Wu, S. Bony, The role of large-scale atmospheric circulation in the relationship between tropical convection and sea surface temperature. *J. Clim.* **10**, 381–392 (1997).
36. J. F. Dutton, C. J. Poulsen, J. L. Evans, The effect of global climate change on the regions of tropical convection in CSM1. *Geophys. Res. Lett.* **27**, 3049–3052 (2000).
37. N. C. Johnson, S.-P. Xie, Changes in the sea surface temperature threshold for tropical convection. *Nat. Geosci.* **3**, 842–845 (2010).
38. H. Wang, W. M. Mehta, Decadal variability of the Indo-Pacific warm pool and its association with atmospheric and oceanic variability in the NCEP–NCAR and SODA reanalyses. *J. Clim.* **21**, 5545–5565 (2008).
39. N. A. Rayner, D. E. Parker, E. B. Horton, C. K. Folland, L. V. Alexander, D. P. Rowell, E. C. Kent, A. Kaplan, Global analyses of sea surface temperature, sea ice, and night marine air temperature since the late nineteenth century. *J. Geophys. Res.* **108**, 4407 (2003).
40. T. M. Smith, R. W. Reynolds, T. C. Peterson, J. Lawrimore, Improvements to NOAA's historical merged land–ocean surface temperature analysis (1880–2006). *J. Clim.* **21**, 2283–2296 (2008).
41. R. F. Adler, G. J. Huffman, A. Chang, R. Ferraro, P.-P. Xie, J. Janowiak, B. Rudolf, U. Schneider, S. Curtis, D. Bolvin, A. Gruber, J. Susskind, P. Arkin, E. Nelkin, The Version-2 Global Precipitation Climatology Project (GPCP) Monthly Precipitation Analysis (1979–present). *J. Hydrometeorol.* **4**, 1147–1167 (2003).
42. A. Ribes, L. Terray, Application of regularised optimal fingerprinting to attribution. Part II: Application to global near-surface temperature. *Clim. Dyn.* **41**, 2837–2853 (2013).
43. M. R. Allen, S. F. B. Tett, Checking for model consistency in optimal fingerprinting. *Clim. Dyn.* **15**, 419–434 (1999).

Acknowledgments: We acknowledge the World Climate Research Programme's Working Group on Coupled Modelling, which is responsible for CMIP, and we thank the climate modeling groups for producing and making their model output available. For CMIP, the U.S. Department of Energy's Program for Climate Model Diagnosis and Intercomparison provided coordinating support and led the development of software infrastructure in partnership with the Global Organization for Earth System Science Portals. **Funding:** E.W. was supported by the Brain Pool Program through the Korean Federation of Science and Technology Societies funded by the Ministry of Science, ICT and Future Planning (141S-1-3-0023). S.-K.M. was supported by the Korea Meteorological Administration Research and Development Program under grant KMIPA 2015-2082. W.C. was supported by the Australian Climate Change Science Programme. **Author contributions:** S.-K.M. and E.W. designed the research and directed the analysis. E.W. conducted the analysis and wrote the draft of the paper. S.-K.M., E.W., W.C., and F.W.Z. interpreted the results and improved the paper. Y.-H.K. and D.L. collected and processed the model data. **Competing interests:** The authors declare that they have no competing interests. **Data and materials availability:** All data used to obtain the conclusions in this paper are available in the public data archive for each data set as cited in the paper and the Supplementary Materials. Additional data related to this paper may be requested from the authors.

Submitted 27 November 2015
Accepted 3 June 2016
Published 1 July 2016
10.1126/sciadv.1501719

Citation: E. Weller, S.-K. Min, W. Cai, F. W. Zwiers, Y.-H. Kim, D. Lee, Human-caused Indo-Pacific warm pool expansion. *Sci. Adv.* **2**, e1501719 (2016).

Science Advances

Human-caused Indo-Pacific warm pool expansion

Evan Weller, Seung-Ki Min, Wenju Cai, Francis W. Zwiers, Yeon-Hee Kim and Donghyun Lee

Sci Adv **2** (7), e1501719.
DOI: 10.1126/sciadv.1501719

Science Advances (ISSN 2375-2548) is published by the American Association for the Advancement of Science, 1200 New York Avenue NW, Washington, DC 20005. The title *Science Advances* is a registered trademark of AAAS.